Available online at www.sciencedirect.com
ScienceDirect
Comput. Methods Appl. Mech. Engrg. 327 (2017) 503–521
Computer methods in applied mechanics and engineering
www.elsevier.com/locate/cma

On the dynamics and breakup of quadcopters using a discrete element method framework

T.I. Zohdi

Department of Mechanical Engineering, University of California, , Berkeley, CA, 94720-1740, USA

Available online 20 July 2017

Abstract

Unmanned Aerial Vehicles (UAVs), in particular quadcopters, have become extremely prevalent, driven by their low cost and ease of control. Unfortunately, privacy concerns related to the ubiquity of UAVs have prompted substantial citizen interest in the shooting down of UAVs that trespass onto their property, although the legality thereof is unclear. In this work, the dynamical response of a quadcopter to a series of randomly external impulses, which could be generated by objects launched toward the UAV, such shotgun pellets, etc., is formulated. A Discrete Element Method (DEM) is developed to describe the breakup of the quadcopter, in conjunction with a staggered implicit time-stepping scheme. The use of DEM allows for fragmentation of the quadcopter and also to compute the trajectories and distribution of the resulting debris field.

Keywords: Quadcopters; Modeling; Simulation

1. Introduction

Unmanned Air Vehicles (UAVs), specifically quadcopters and multicopters, have become widely used worldwide for recreational and technological reasons. *For example, the dramatic increase in inexpensive Unmanned Aerial Vehicle (UAV) and camera technology has made the real-time mapping of areas struck by disasters, such as fires, earthquakes, tsunamis, etc., a reality.* For example, the optimal deployment of multiple UAVs for rapid mapping and assessment before and after a multi-location disaster, such as an earthquake, requires detailed inspection of infrastructures (roads, bridges, pipelines, power grids and water systems) in difficult to reach locations. Proper deployment of UAVs promises to provide first responders to disasters with timely information in multiple locations. Critical infrastructure is now multi-faceted, comprising, water grids, power, traffic, etc., and in many municipalities UAV mapping is being proposed, and in some cases already deployed. Technological advances and societal changes such as massive numbers of cost-effective UAVs are now game-changers in terms of the ability to both (1) monitor and control events in a disaster and (2) to facilitate long-term planning. (See Fig. 1.)

Unfortunately, the proliferation of these small flying vehicles, and the resulting concerns regarding invasion of privacy, has led to many cases of individuals attempting to shoot down UAVs that enter into the airspace above their

E-mail address: zohdi@berkeley.edu.

http://dx.doi.org/10.1016/j.cma.2017.07.009
0045-7825/

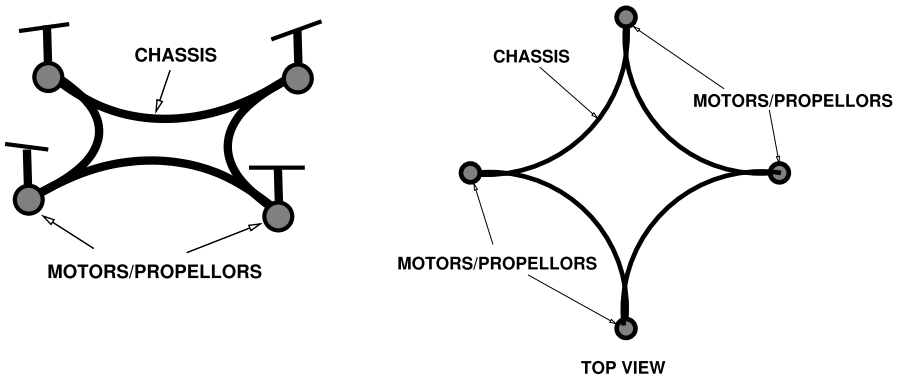

Fig. 1. Prototypical design of a quadcopter. The propellors remain perpendicular to the chassis and provide thrust.

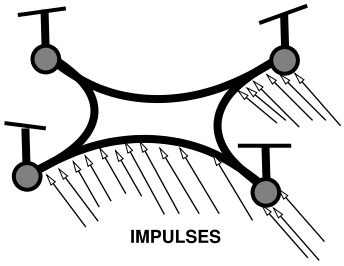

Fig. 2. A quadcopter hit with external impulses.

property. This is technically illegal according to FAA regulations, primarily because it can harm individuals and property below from the scattered debris. It is estimated that UAVs are shot down in the US at a rate of one UAV per month (in 2016). The legality of shooting down a UAV is complex, and determined in part by the height at which the UAV was flying at the time.[1] To the knowledge of the author, no works have explored the dynamical response and possible breakup of a UAV being shot at, for example, by a shotgun.

In this paper, the dynamical response of a quadcopter to a series of random external impulses (Fig. 2), such as from shotgun pellets, is formulated using a Discrete Element Method. The use of DEM allows for the fragmentation of the quadcopter and allows one to also compute the trajectories and distribution of the debris field. Various initial conditions can be tested which can *potentially aid* in settling disputes, for example by determining the height and location of the UAV prior to it being shot down, and correlating the simulated and observed debris field.

2. Generation of a cluster of bonded elements/particles

To generate the quadcopter body, we insert particles within an envelope/grid intersection (Fig. 3). For example, a convenient, easy to parametrize envelope is given by sweeping through a rectangular parallelepiped of $(\pm R_1, \pm R_2, \pm R_3)$ and checking the intersection of the hull envelope equation, for example given by a generalized ellipsoidal equation:

$$\frac{|x_1 - x_{1o}|^{p_1}}{R_1} + \frac{|x_2 - x_{2o}|^{p_1}}{R_2} + \frac{|x_3 - x_{3o}|^{p_3}}{R_3} \leq 1, \tag{2.1}$$

where (x_1, x_2, x_3) are the coordinates of the DEM particles,(x_1, x_2, x_3) are the coordinates of center of the chassis, (R_1, R_2, R_3) are the generalized radii and (p_1, p_2, p_3) are exponents of the generalized ellipsoid, with a box of discrete element "subbox" positions (Fig. 3). Where there is an intersection, a particle is placed in the subbox. The particles are initially rigidly bonded together, but may become dislodged due to external forces (discussed later in the presentation).

[1] See https://www.yahoo.com/news/whos-sky-anyway-u-drone-case-tests-rights-132753742.html.

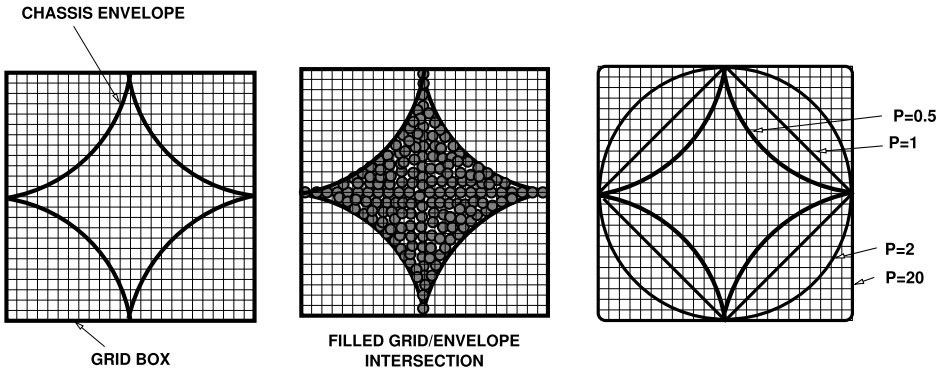

Fig. 3. Generating a UAV hull with discrete elements. This is achieved by sweeping through a rectangular parallelepiped of $(\pm R_1, \pm R_2, \pm R_3)$ and checking the intersection of the hull envelope equation above with a box of discrete element position subboxes (left). Where there is an intersection, and particle is placed in the subbox (middle). A generalized ellipsoidal equation (Eq. (2.1)) is used where for exponent values of (p_1, p_2, p_3) equal to two, we generate a familiar ellipsoid, for values less than one we generate involute (nonconvex shapes), and for exponent values of (p_1, p_2, p_3) greater than two, we generate a box-like shapes (right).

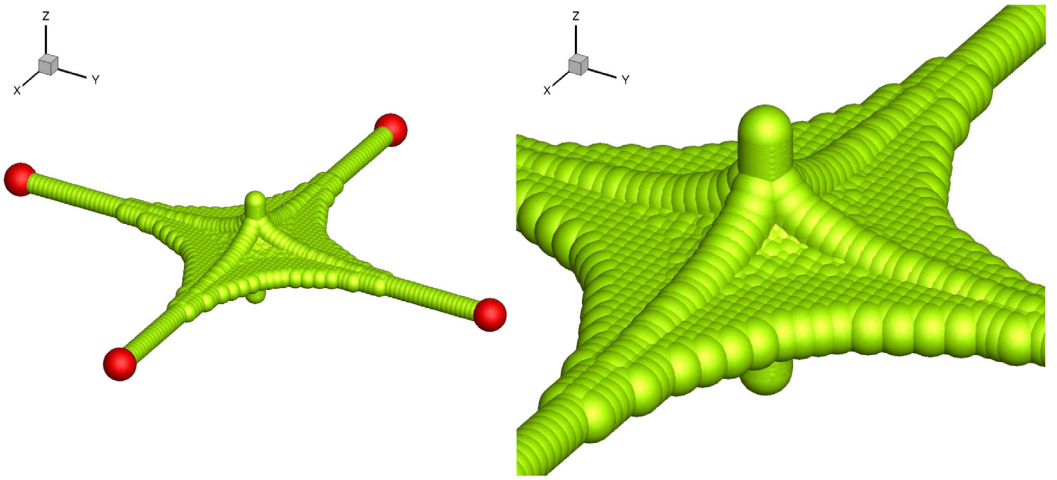

Fig. 4. For $(p_1, p_2, p_3) = (0.2, 0.2, 0.2)$. Right: A DEM generated UAV frame. Left: A zoom on the *locations* of the DEM particles. The particles are bound by the mathematical dynamics-constraints to move collectively as a rigid body (group translation and rotation), until a particle is dislodged by an impulse. If it is dislodged, it moves according to its own dynamics.

For exponent values of (p_1, p_2, p_3) equal to two, we generate a familiar ellipsoid, for values less than one we generate involute (nonconvex shapes, Fig. 3), and for exponent values of (p_1, p_2, p_3) greater than two, we generate a box-like shapes.

3. Dynamics of general rigid clusters of DEM particles

In order to make the analysis general, we consider rigid clusters of DEM particles. Later we will tailor the cluster to specific UAV designs. We consider the DEM cluster to be already formed, with particles rigidly bonded together. Later, we will allow particles to become dislodged from the cluster. Consider a collection of rigidly-bonded particles, $i = 1, 2, \ldots, N_c$, in a cluster. The individual particle dynamics are described by (which leads to a coupled system)

$$m_i \ddot{\mathbf{r}}_i = m_i \dot{\mathbf{v}}_i = \underbrace{\boldsymbol{\Psi}_i^{tot}}_{\text{total forces}} = \underbrace{\boldsymbol{\Psi}_i^{int}}_{\text{internal}} + \underbrace{\boldsymbol{\Psi}_i^{ext}}_{\text{external}}, \tag{3.1}$$

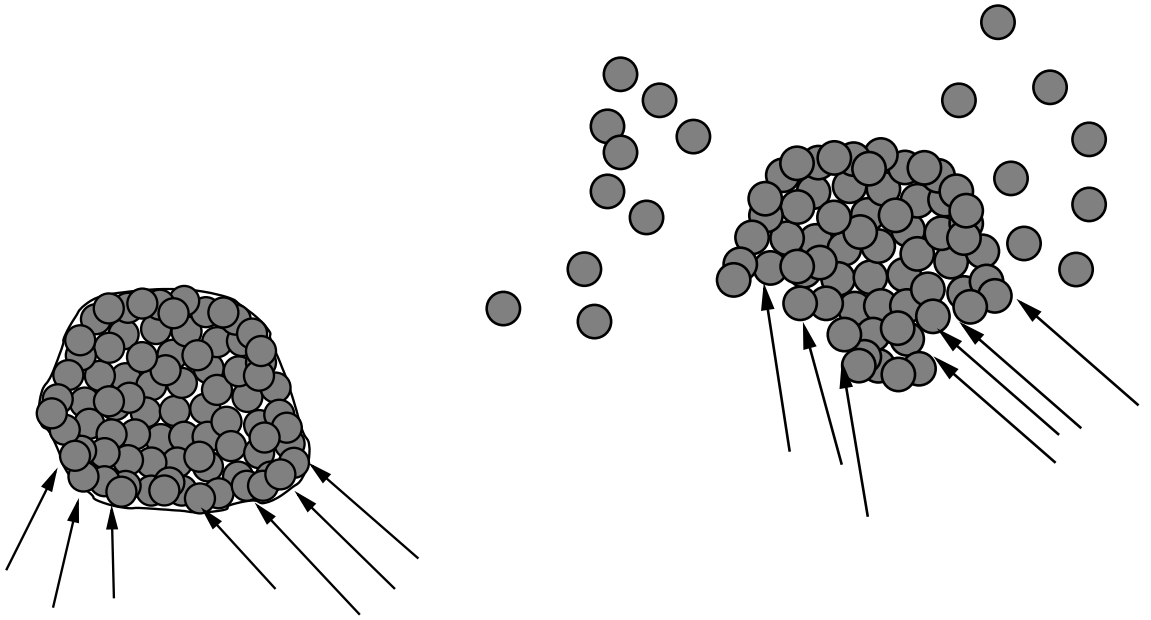

Fig. 5. Left: A collection of DEM particles (a "cluster") that are rigidly bonded together. Right: Motion and breakup of a cluster from impulses.

where m_i is the mass of the ith particle, $\boldsymbol{r}_i$ is the position vector, $\boldsymbol{v}_i$ is the particle velocity, $\boldsymbol{\Psi}_i^{ext}$ is an external force field and $\boldsymbol{\Psi}_i^{int}$ is the sum of the internal (equal in magnitude and opposite in direction) forces acting on the ith particle, due to other particles in the system ("internal" particle-to-particle bonding forces, contact forces etc. (See Fig. 5.)

4. Group dynamics of a rigidly bound collection of particles

When we consider a collection of particles that are bound together as a rigid body,

Because internal forces between particles within in the system are opposite in direction and equal in magnitude, the specific character of the internal particle-to-particle bonding forces is not relevant to the overall system dynamics,

$$\sum_{i=1}^{N_c} \left(\boldsymbol{\Psi}_i^{ext} + \boldsymbol{\Psi}_i^{int} \right) = \sum_{i=1}^{N_c} \boldsymbol{\Psi}_i^{ext} + \underbrace{\sum_{i=1}^{N_c} \boldsymbol{\Psi}_i^{int}}_{=\boldsymbol{0}} = \sum_{i=1}^{N_c} \boldsymbol{\Psi}_i^{ext} \stackrel{\text{def}}{=} \boldsymbol{\Psi}^{EXT}, \tag{4.1}$$

where $\boldsymbol{\Psi}^{EXT}$ is the overall external force acting on the cluster and N_c are the number of particles in the DEM cluster. The position vector of the center of mass of the system is given by

$$\boldsymbol{r}_{cm} \stackrel{\text{def}}{=} \frac{\sum_{i=1}^{N_c} m_i \boldsymbol{r}_i}{\sum_{i=1}^{N_c} m_i} = \frac{1}{\mathcal{M}} \sum_{i=1}^{N_c} m_i \boldsymbol{r}_i, \tag{4.2}$$

where $\mathcal{M}$ is the total system mass. A decomposition of the position vector for particle i, of the form $\boldsymbol{r}_i = \boldsymbol{r}_{cm} + \boldsymbol{r}_{cm \to i}$, allows the linear momentum of the system of particles ($\boldsymbol{G}$) to be written as

$$\sum_{i=1}^{N_c} \underbrace{m_i \dot{\boldsymbol{r}}_i}_{\boldsymbol{G}_i} = \sum_{i=1}^{N_c} m_i (\dot{\mathbf{r}}_{cm} + \dot{\mathbf{r}}_{cm \to i}) = \sum_{i=1}^{N_c} m_i \dot{\mathbf{r}}_{cm} = \dot{\mathbf{r}}_{cm} \sum_{i=1}^{N_c} m_i = \mathcal{M} \dot{\mathbf{r}}_{cm} \stackrel{\text{def}}{=} \boldsymbol{G}_{cm}, \tag{4.3}$$

since $\sum_{i=1}^{N_c} m_i \dot{\mathbf{r}}_{cm\to i} = \mathbf{0}$. Furthermore, $\dot{\mathbf{G}}_{cm} = \mathcal{M}\ddot{\mathbf{r}}_{cm}$, thus

$$\dot{\mathbf{G}}_{cm} = \mathcal{M}\ddot{\mathbf{r}}_{cm} = \sum_{i=1}^{N_c} \boldsymbol{\psi}_i^{ext} \stackrel{\text{def}}{=} \boldsymbol{\Psi}^{EXT}. \tag{4.4}$$

The angular momentum relative to the center of mass can be written as (utilizing $\dot{\mathbf{r}}_i = \boldsymbol{v}_i = \boldsymbol{v}_{cm} + \boldsymbol{v}_{cm\to i}$)

$$\sum_{i=1}^{N_c} \boldsymbol{H}_{cm\to i} = \sum_{i=1}^{N_c} (\boldsymbol{r}_{cm\to i} \times m_i \boldsymbol{v}_{cm\to i}) = \sum_{i=1}^{N_c} (\boldsymbol{r}_{cm\to i} \times m_i (\boldsymbol{v}_i - \boldsymbol{v}_{cm})) \tag{4.5}$$

$$= \sum_{i=1}^{N_c} (m_i \boldsymbol{r}_{cm\to i} \times \boldsymbol{v}_i) - \left(\underbrace{\sum_{i=1}^{N_c} m_i \boldsymbol{r}_{cm\to i}}_{=0} \right) \times \boldsymbol{v}_{cm} = \boldsymbol{H}_{cm}, \tag{4.6}$$

for a rigid body. Since $\boldsymbol{v}_{cm\to i} = \boldsymbol{\omega} \times \boldsymbol{r}_{cm\to i}$

$$\boldsymbol{H}_{cm} = \sum_{i=1}^{N_c} \boldsymbol{H}_{cm\to i} = \sum_{i=1}^{N_c} m_i (\boldsymbol{r}_{cm\to i} \times \boldsymbol{v}_{cm\to i}) = \sum_{i=1}^{N_c} m_i (\boldsymbol{r}_{cm\to i} \times (\boldsymbol{\omega} \times \boldsymbol{r}_{cm\to i})). \tag{4.7}$$

Decomposing the relative position vector into its components

$$\boldsymbol{r}_{cm\to i} = \boldsymbol{r}_i - \boldsymbol{r}_{cm} = \hat{x}_{i1}\boldsymbol{e}_1 + \hat{x}_{i2}\boldsymbol{e}_2 + \hat{x}_{i3}\boldsymbol{e}_3, \tag{4.8}$$

where $\hat{x}_{i1}$, $\hat{x}_{i2}$ and $\hat{x}_{i3}$ are the coordinates of the mass points measured *relative to the center of mass*, and expanding the angular momentum expression, yields

$$H_1 = \omega_1 \sum_{i=1}^{N_c} (\hat{x}_{i2}^2 + \hat{x}_{i3}^2)\, m_i - \omega_2 \sum_{i=1}^{N_c} \hat{x}_{i1}\hat{x}_{i2}\, m_i - \omega_3 \sum_{i=1}^{N_c} \hat{x}_{i1}\hat{x}_{i3}\, m_i \tag{4.9}$$

and

$$H_2 = -\omega_1 \sum_{i=1}^{N_c} \hat{x}_{i1}\hat{x}_{i2}\, m_i + \omega_2 \sum_{i=1}^{N_c} (\hat{x}_{i1}^2 + \hat{x}_{i3}^2)\, m_i - \omega_3 \sum_{i=1}^{N_c} \hat{x}_{i2}\hat{x}_{i3}\, m_i \tag{4.10}$$

and

$$H_3 = -\omega_1 \sum_{i=1}^{N_c} \hat{x}_{i1}\hat{x}_{i3}\, m_i - \omega_2 \sum_{i=1}^{N_c} \hat{x}_{i2}\hat{x}_{i3}\, m_i + \omega_3 \sum_{i=1}^{N_c} (\hat{x}_{i1}^2 + \hat{x}_{i2}^2)\, m_i, \tag{4.11}$$

which can be concisely written as

$$\boldsymbol{H}_{cm} = \overline{\boldsymbol{\mathcal{I}}} \cdot \boldsymbol{\omega}, \tag{4.12}$$

where we define the moments of inertia with respect to the center of mass

$$\overline{\mathcal{I}}_{11} = \sum_{i=1}^{N_c} (\hat{x}_{i2}^2 + \hat{x}_{i3}^2)\, m_i, \qquad \overline{\mathcal{I}}_{22} = \sum_{i=1}^{N_c} (\hat{x}_{i1}^2 + \hat{x}_{i3}^2)\, m_i, \qquad \overline{\mathcal{I}}_{33} = \sum_{i=1}^{N_c} (\hat{x}_{i1}^2 + \hat{x}_{i2}^2)\, m_i, \tag{4.13}$$

$$\overline{\mathcal{I}}_{12} = \overline{\mathcal{I}}_{21} = -\sum_{i=1}^{N_c} \hat{x}_{i1}\hat{x}_{i2}\, m_i, \qquad \overline{\mathcal{I}}_{23} = \overline{\mathcal{I}}_{32} = -\sum_{i=1}^{N_c} \hat{x}_{i2}\hat{x}_{i3}\, m_i, \qquad \overline{\mathcal{I}}_{13} = \overline{\mathcal{I}}_{31} = -\sum_{i=1}^{N_c} \hat{x}_{i1}\hat{x}_{i3}\, m_i, \tag{4.14}$$

or explicitly

$$\overline{\boldsymbol{\mathcal{I}}} = \begin{bmatrix} \overline{\mathcal{I}}_{11} & \overline{\mathcal{I}}_{12} & \overline{\mathcal{I}}_{13} \\ \overline{\mathcal{I}}_{21} & \overline{\mathcal{I}}_{22} & \overline{\mathcal{I}}_{23} \\ \overline{\mathcal{I}}_{31} & \overline{\mathcal{I}}_{32} & \overline{\mathcal{I}}_{33} \end{bmatrix}. \tag{4.15}$$

The particles' own inertia contribution about their respective mass-centers to the overall moment of inertia of the agglomerated body can be described by the Huygens–Steiner (generalized "parallel axis" theorem) formula $(p, s = 1, 2, 3)$

$$\bar{\mathcal{I}}_{ps} = \sum_{i=1}^{N_c} \left(\bar{\mathcal{I}}^i_{ps} + m_i (\|\boldsymbol{r}_i - \boldsymbol{r}_{cm}\|^2 \delta_{ps} - \hat{x}_{ip}\hat{x}_{is}) \right). \tag{4.16}$$

For a spherical particle, $\bar{\mathcal{I}}^i_{pp} = \frac{2}{5} m_i R_i^2$, and for $p \neq s$, $\bar{\mathcal{I}}^i_{ps} = 0$ (no products of inertia), R_i being the particle radius.[2] Finally, for the derivative of the angular momentum , utilizing $\ddot{\mathbf{r}}_i = \boldsymbol{a}_i = \boldsymbol{a}_{cm} + \boldsymbol{a}_{cm \to i}$, we obtain

$$\dot{\mathbf{H}}^{rel}_{cm} = \sum_{i=1}^{N_c} (\boldsymbol{r}_{cm \to i} \times m_i \boldsymbol{a}_{cm \to i}) = \sum_{i=1}^{N_c} (\boldsymbol{r}_{cm \to i} \times m_i (\boldsymbol{a}_i - \boldsymbol{a}_{cm})) \tag{4.17}$$

$$= \sum_{i=1}^{N_c} (m_i \boldsymbol{r}_{cm \to i} \times \boldsymbol{a}_i) \underbrace{- (\sum_{i=1}^{N_c} m_i \boldsymbol{r}_{cm \to i})}_{=0} \times \boldsymbol{a}_{cm} = \dot{\mathbf{H}}_{cm}, \tag{4.18}$$

and consequently

$$\dot{\mathbf{H}}_{cm} = \frac{d(\overline{\boldsymbol{\mathcal{I}}} \cdot \boldsymbol{\omega})}{dt} = \sum_{i=1}^{N_c} \boldsymbol{r}_{cm \to i} \times \boldsymbol{\psi}^{ext}_i \stackrel{\text{def}}{=} \boldsymbol{M}^{EXT}_{cm}, \tag{4.19}$$

where $\boldsymbol{M}^{EXT}_{cm}$ is the total external moment about the center of mass.

5. Numerical methods for the dynamics of a DEM cluster

We now treat the dynamics of a cluster numerically. We first focus on the translational motion of the center of mass, and then turn to the rotational contribution.

5.1. DEM cluster translational contribution

The translational component of the center of mass can be written as

$$\mathcal{M} \ddot{\mathbf{r}}_{cm} = \mathcal{M} \dot{\mathbf{v}}_{cm} = \boldsymbol{\Psi}^{EXT}. \tag{5.1}$$

A trapezoidal time-stepping rule is used, whereby at some intermediate moment in time $t \leq t + \phi \Delta t \leq t + \Delta t$ $(0 \leq \phi \leq 1)$

$$\dot{\mathbf{v}}_{cm}(t + \phi \Delta t) \approx \frac{\boldsymbol{v}_{cm}(t + \Delta t) - \boldsymbol{v}_{cm}(t)}{\Delta t} \tag{5.2}$$

$$= \frac{1}{\mathcal{M}(t + \phi \Delta t)} \boldsymbol{\Psi}^{EXT}(t + \phi \Delta t) \tag{5.3}$$

$$\approx \frac{1}{\mathcal{M}(t + \phi \Delta t)} \left(\phi \, \boldsymbol{\Psi}^{EXT}(t + \Delta t) + (1 - \phi) \, \boldsymbol{\Psi}^{EXT}(t) \right), \tag{5.4}$$

where $\mathcal{M}(t + \phi \Delta t) \approx \phi \mathcal{M}(t + \Delta t) + (1 - \phi)\mathcal{M}(t)$, leading to

$$\boldsymbol{v}_{cm}(t + \Delta t) = \boldsymbol{v}_{cm}(t) + \frac{\Delta t}{\mathcal{M}(t + \phi \Delta t)} \left(\phi \, \boldsymbol{\Psi}^{EXT}(t + \Delta t) + (1 - \phi) \, \boldsymbol{\Psi}^{EXT}(t) \right). \tag{5.5}$$

[2] If the particles are sufficiently small, each particle's own moment inertia (about its own center) is insignificant, leading to $\bar{\mathcal{I}}_{ps} = \sum_{i=1}^{N_c} m_i (\|\boldsymbol{r}_i - \boldsymbol{r}_{cm}\|^2 \delta_{ps} - \hat{x}_{ip}\hat{x}_{is})$.

For the position, we have

$$\dot{\mathbf{r}}_{cm}(t+\phi\Delta t) \approx \frac{\boldsymbol{r}_{cm}(t+\Delta t)-\boldsymbol{r}_{cm}(t)}{\Delta t} \approx \boldsymbol{v}_{cm}(t+\phi\Delta t) \approx (\phi \boldsymbol{v}_{cm}(t+\Delta t)+(1-\phi)\boldsymbol{v}_{cm}(t)) \,, \tag{5.6}$$

leading to

$$\boldsymbol{r}_{cm}(t+\Delta t) = \boldsymbol{r}_{cm}(t) + \Delta t\, (\phi \boldsymbol{v}_{cm}(t+\Delta t)+(1-\phi)\boldsymbol{v}_{cm}(t)) \,. \tag{5.7}$$

5.2. Rotational dynamics

The quadcopter's angular velocity and rotation are determined in a similar manner by integrating the equations for an angular momentum balance

$$\dot{\mathbf{H}}_{cm} = \frac{d(\overline{\boldsymbol{\mathcal{I}}}\cdot\boldsymbol{\omega})}{dt} = \boldsymbol{M}_{cm}^{EXT}, \tag{5.8}$$

where $\overline{\boldsymbol{\mathcal{I}}}$ is the mass moment of the quadcopter, $\boldsymbol{\omega}$ is the angular velocity and $\boldsymbol{M}_{cm}^{EXT}$ is the sum of all moment contributions external to the quadcopter, around its center of mass. We remark that there are essentially two possible approaches to compute the rotational dynamics; either (1) an inertially-fixed frame or (2) a body-fixed frame. For the discrete element approach, it is advantageous to use a inertially-fixed frame.[3] The procedure is, within a time step, to decompose an increment of motion into a rigid body translation and rotation about the center of mass. The rotation is determined by solving for the angular velocity and the subsequent incremental rotation of the body around the axis of rotation, which is aligned with the angular velocity vector direction. This leads to a coupled set of nonlinear equations which are solved iteratively.

In a fixed frame of reference the angular momentum can be written as

$$\dot{\mathbf{H}}_{cm} = \frac{d(\overline{\boldsymbol{\mathcal{I}}}\cdot\boldsymbol{\omega})}{dt} = \boldsymbol{M}_{cm}^{EXT}. \tag{5.9}$$

$\overline{\boldsymbol{\mathcal{I}}}$ is implicitly dependent on $\boldsymbol{\omega}(t)$, leading to a coupled system of nonlinear ODE's. These will be solved iteratively. Eq. (5.9) is discretized by a trapezoidal scheme

$$\frac{d(\overline{\boldsymbol{\mathcal{I}}}\cdot\boldsymbol{\omega})}{dt}|_{t+\phi\Delta t} = \frac{(\overline{\boldsymbol{\mathcal{I}}}\cdot\boldsymbol{\omega})|_{t+\Delta t}-(\overline{\boldsymbol{\mathcal{I}}}\cdot\boldsymbol{\omega})|_{t}}{\Delta t} \tag{5.10}$$

thus leading to

$$(\overline{\boldsymbol{\mathcal{I}}}\cdot\boldsymbol{\omega})|_{t+\Delta t} = (\overline{\boldsymbol{\mathcal{I}}}\cdot\boldsymbol{\omega})|_{t} + \Delta t \boldsymbol{M}_{cm}^{EXT}(t+\phi\Delta t). \tag{5.11}$$

Solving for $\boldsymbol{\omega}(t+\Delta t)$ yields

$$\boldsymbol{\omega}(t+\Delta t) = \left(\overline{\boldsymbol{\mathcal{I}}}(t+\Delta t)\right)^{-1}\cdot\left((\overline{\boldsymbol{\mathcal{I}}}\cdot\boldsymbol{\omega})|_{t} + \Delta t \boldsymbol{M}_{cm}^{EXT}(t+\phi\Delta t)\right), \tag{5.12}$$

where

$$\boldsymbol{M}_{cm}^{EXT}(t+\phi\Delta t) \approx \phi \boldsymbol{M}_{cm}^{EXT}(t+\Delta t) + (1-\phi)\boldsymbol{M}_{cm}^{EXT}(t) \tag{5.13}$$

which yields an implicit nonlinear equation, of the form $\boldsymbol{\omega}(t+\Delta t) = \mathcal{F}(\boldsymbol{\omega}(t+\Delta t))$, since $\overline{\boldsymbol{\mathcal{I}}}(t+\Delta t)$, due to the body's rotation. An iterative, implicit, solution scheme may be written as follows for $K = 1, 2...$

$$\boldsymbol{\omega}^{K+1}(t+\Delta t) = \left(\overline{\boldsymbol{\mathcal{I}}}^{K}(t+\Delta t)\right)^{-1}\cdot\left((\overline{\boldsymbol{\mathcal{I}}}\cdot\boldsymbol{\omega})|_{t} + \Delta t \boldsymbol{M}_{cm}^{EXT,K}(t+\phi\Delta t)\right), \tag{5.14}$$

[3] For a body-fixed formulation, see Powell and Zohdi [1].

where $\overline{\mathcal{I}}^K(t+\Delta t)$ can be re-computed from the previous formulas.[4] After the update for $\boldsymbol{\omega}^{K+1}(t+\Delta t)$ has been computed (utilizing the $\overline{\mathcal{I}}^K(t+\Delta t)$ from the previous iteration), the rotation of the body about the center of mass can be determined.

5.3. Iterative superposition scheme-including loss of dislodged particles

The total velocity of any particle can be decomposed into the velocity of the center of mass of the entire object and the rotation of the particle relative to the center of mass:

$$\boldsymbol{v}_i = \boldsymbol{v}_{cm} + (\boldsymbol{v}_i - \boldsymbol{v}_{cm}) = \boldsymbol{v}_{cm} + \boldsymbol{v}_{cm\rightarrow i} = \boldsymbol{v}_{cm} + \boldsymbol{\omega} \times (\boldsymbol{r}_{cm} - \boldsymbol{r}_i) = \boldsymbol{v}_{cm} + \boldsymbol{\omega} \times \boldsymbol{r}_{cm\rightarrow i}. \tag{5.15}$$

Explicitly, the overall motion for the bonded particles is computed by $\boldsymbol{r}_i = \boldsymbol{r}_{cm} + \boldsymbol{\omega} \times (\boldsymbol{r}_i - \boldsymbol{r}_{cm})$, sequentially by computing:

- $\boldsymbol{C}_1 = \phi \boldsymbol{v}_{cm}(t+\Delta t) + (1-\phi)\boldsymbol{v}_{cm}(t)$,
- $\boldsymbol{C}_2 = \phi \boldsymbol{\omega}(t+\Delta t) + (1-\phi)\boldsymbol{\omega}(t)$,
- $\boldsymbol{C}_3 = \phi \boldsymbol{r}_{cm}(t+\Delta t) + (1-\phi)\boldsymbol{r}_{cm}(t)$,
- $\boldsymbol{C}_4 = \phi \boldsymbol{r}_i(t+\Delta t) + (1-\phi)\boldsymbol{r}_i(t) - \boldsymbol{C}_3$,
- $\boldsymbol{C}_5 = \boldsymbol{C}_2 \times \boldsymbol{C}_4$,
- $\boldsymbol{r}_i(t+\Delta t) = \boldsymbol{r}_i + \Delta t(\boldsymbol{C}_1 + \boldsymbol{C}_5)$.

For particles that have broken off, one calculates

- $\boldsymbol{v}_i(t+\Delta t) = \boldsymbol{v}_i(t) + \frac{\Delta t}{m_i}(\boldsymbol{p}_i(t+\delta t) - m_i \boldsymbol{g})$,
- $\boldsymbol{r}_i(t+\Delta t) = \boldsymbol{r}_i(t) + \Delta t \phi \boldsymbol{v}_i(t+\Delta t) + (1-\phi)\boldsymbol{v}_i(t)$,

where $\boldsymbol{p}_i$ is the impulse on the loose particle that was bonded to the rigid body. We assume that a portion of the impulse that hits the rigid body is absorbed by the body, and if the particle is dislodged a portion acts on the loose particle. The criteria used is a rather simple one. One simply checks the magnitude of impulse that the particle experiences, and if the magnitude exceeds a threshold, the particle is deemed "dislodged" and moves according to its own dynamics. This is a complex fragmentation process that is beyond the scope of this paper. We refer the reader to Zohdi [2–7] for details. This entire system is solved recursively within each time step, thus forming a fixed point iteration of the form:

$$\boldsymbol{r}_i^{K+1}(t+\Delta t) = \boldsymbol{G}(\boldsymbol{r}_i^K(t+\Delta t)) + \boldsymbol{R}. \tag{5.16}$$

The convergence of such a scheme scales with the time-step size. For sufficiently small sizes, the scheme converges quite quickly and is second-order accurate.

Remark. Adaptive time-stepping schemes are also possible (see Appendix B).

5.4. Algorithmic procedure

The overall procedure is as follows, at time t:

1. Generate the quadcopter body by inserting particles within the envelope/grid interaction (Fig. 3):
$$\frac{|x_1 - x_{1o}|^{p_1}}{R_1} + \frac{|x_2 - x_{2o}|^{p_1}}{R_2} + \frac{|x_3 - x_{3o}|^{p_3}}{R_3} \leq 1. \tag{5.17}$$
Also place extra masses in the locations for the motors.
2. Set initial conditions, if $t = 0$.
3. Compute the thrust of the motors (orthogonal to the quadcopter body).
4. Compute the new position of the center of mass.

[4] One may view the overall process as a fixed-point calculation of the form $\boldsymbol{\omega}^{K+1}(t+\Delta t) = \mathcal{F}(\boldsymbol{\omega}^K(t+\Delta t))$.

5. Compute (iteratively) the positions of the particles in the body $\boldsymbol{r}_i^K(t+\Delta t)$, $K = 1, 2, \ldots$.:

$$\|\boldsymbol{r}_i^{K+1}(t+\Delta t) - \boldsymbol{r}_i^K(t+\Delta t)\| \leq TOL\|\boldsymbol{r}_i^{K+1}(t+\Delta t)\|. \tag{5.18}$$

This requires computation of the position of the center of mass, the rotation of the body, and the calculation of the positions of the particles within the iterations:

(a) Compute/update: $\boldsymbol{v}_{cm}^{K+1}(t+\Delta t) = \boldsymbol{v}_{cm}(t) + \frac{\Delta t}{\mathcal{M}(t+\phi\Delta t)}\left(\phi\,\boldsymbol{\Psi}^{K+1,EXT}(t+\Delta t) + (1-\phi)\,\boldsymbol{\Psi}^{EXT}(t)\right)$.
(b) Compute/update: $\boldsymbol{r}_{cm}^{K+1}(t+\Delta t) = \boldsymbol{r}_{cm}(t) + \Delta t\,(\phi\boldsymbol{v}_{cm}(t+\Delta t) + (1-\phi)\boldsymbol{v}_{cm}(t))$.
(c) Compute/update: $\boldsymbol{M}_{cm}^{EXT}(t+\phi\Delta t) \approx \phi\boldsymbol{M}_{cm}^{EXT}(t+\Delta t) + (1-\phi)\boldsymbol{M}_{cm}^{EXT}(t)$,
(d) Compute/update: $\boldsymbol{\omega}^{K+1}(t+\Delta t) = \left(\overline{\mathcal{I}}^K(t+\Delta t)\right)^{-1}\cdot\left((\overline{\mathcal{I}}\cdot\boldsymbol{\omega})|_t + \Delta t\boldsymbol{M}_{cm}^{EXT,K}(t+\phi\Delta t)\right)$,
(e) Compute/update: $\boldsymbol{v}_i = \boldsymbol{v}_{cm} + \boldsymbol{\omega}\times\boldsymbol{r}_{cm\to i}$
(f) Compute/update: $\boldsymbol{r}_i(t+\Delta t) = \boldsymbol{r}_i + \Delta t(\boldsymbol{C}_1 + \boldsymbol{C}_5)$,
(g) Repeat steps (a)-(f) until Eq. (5.18) is satisfied.

6. After convergence within a time step, for particles that have broken off, calculate
(a) $\boldsymbol{v}_i(t+\Delta t) = \boldsymbol{v}_i(t) + \frac{\Delta t}{m_i}(\boldsymbol{p}_i(t+\delta t) - m_i\boldsymbol{g})$,
(b) $\boldsymbol{r}_i(t+\Delta t) = \boldsymbol{r}_i(t) + \Delta t\phi\boldsymbol{v}_i(t+\Delta t) + (1-\phi)\boldsymbol{v}_i(t)$.
7. Increment time forward and repeat the procedure.

Remark. The contact mechanics of dislodged particles with other dislodged material, the remainder of the UAV hull, etc., is outside the scope of the present work. Temporally-adaptive iterative methods maybe needed for more complex particle interaction. We refer the reader to methods found in Zohdi [2–7] that address general systems of this type.

6. Numerical examples

The following simulation parameters were chosen:

- Generation grid for DEM = 100 ×100 ×100, yielding 3751 intersecting sites and hence 3751 particles,
- Total time duration = $T = 4$ s,
- Time step size = $\Delta t = 0.00005$ s,
- Starting position of center of mass, $\boldsymbol{r}_{cm}(t=0) = \boldsymbol{0}$ (horizontal, Fig. 4),
- Time stepping parameter $\phi = 0.5$ (midpoint rule),
- UAV shape exponents $(p_1, p_2, p_3) = (0.2, 0.2, 0.2)$ (Fig. 4),
- Size of UAV: $(R_1, R_2, R_3) = (0.25, 0.25, 0.05)$,
- Mass of the UAV chassis = $M = 1$ kg,
- Starting angular velocity = $\boldsymbol{\omega}(t=0) = \boldsymbol{0}$ rad/s,
- Motor masses: $M_m = 0.25$ kg each,
- Thrust force per motor = 4.55 N (this allows for perfect hovering (propellor thrust balancing gravity) if there is no external impulse),
- Density of the chassis material = $\rho = 1000\ kg/m^3$,
- Motor and propellor radii = 0.025 m,
- Impulse force from each shotgun particle = $(0, -100, 100) \times (1 + a \times \delta)$, a = 0.25, $-1 \leq \delta \leq 1$,
- Number of shotgun blasts = 4 (one every seconds),
- Number of impulses hitting the chassis=100,
- Number of impulses hitting the motors = 5,
- Threshold for dislodging of a particle = 10 N and
- Threshold for dislodging of a motor = 10 N.

If dislodged, 50% of the force is absorbed by the chassis and 50% is absorbed by the particle or motor. If not dislodged, 100% is absorbed by the chassis.

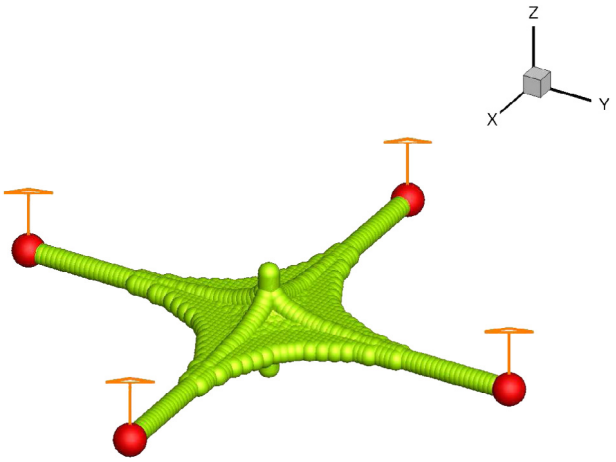

Fig. 6. A hovering UAV in balance between gravity and the propellor thrusts.

6.1. Hovering UAV hit with an impulse

As a first example, we consider an initially hovering (Fig. 6) UAV, with the thrust from the propellors always acting perpendicular to the UAV, being hit repeatedly with a set of random location and random magnitude impulses at a 45 degree angle. In this first example, we do not allow the UAV to break apart. The repeated impulses are strong enough to overturn the UAV, and to destabilize it, as seen in Fig. 7.

6.2. Hovering UAV hit with an impulse and breakup generated debris field

As a second example, we allow the initially hovering (Fig. 6) UAV to break apart, while being hit repeatedly with a set of random location and random magnitude impulses at a 45 degree angle. The repeated impulses are strong enough to break off pieces (particles) as seen in Fig. 8. In Fig. 9, notice that due to the spiraling of the UAV, the debris gets "flung" in different directions, due to being dislodged and released with a combination of the impulse force and the last velocity when attached to the UAV.

7. Extensions and concluding remarks

The following issues represent areas for extending this work:

1. **UAV motor control:** One issue that was not taken into account was adaptive control response of the motors by the UAV operator. For example, Mueller and D'Andrea [8,9], Hehn et al. [10], Houska et al. [11] have investigated the dynamics and control of UAVs, including the ability of a quadcopter to maintain flight despite the complete failure of propellor.
2. **UAV-fragment interaction:** Once a DEM cluster of bonded particles breaks up, the calculation of the interaction of the fragments, with a full contact analysis, is a logical extension of the analysis presented in this work. A relatively straightforward DNS-type formulation of the dynamics of a multi-particulate system, is to track the motion of $i = 1, 2...N$ particles,

$$m_i \ddot{\mathbf{r}}_i = \boldsymbol{\psi}_i^{tot}(\boldsymbol{r}_1, \boldsymbol{r}_2, \ldots, \boldsymbol{r}_{N_p}), \tag{7.1}$$

where $\boldsymbol{r}_i$ is the position vector of the ith particle, $\boldsymbol{\psi}_i^{tot}$ represents all forces acting on particle i The simulation of such flowing particulate systems has been extensively investigated for the last decade by Zohdi [2–7,12–14], employing numerical schemes based on high-performance iterative solvers, sorting–binning for fast inter-particle calculations, Verlet lists, domain decomposition, parallel processing and temporally-adaptive methods, described further in Appendix B. These types of formulations can easily describe the interaction of

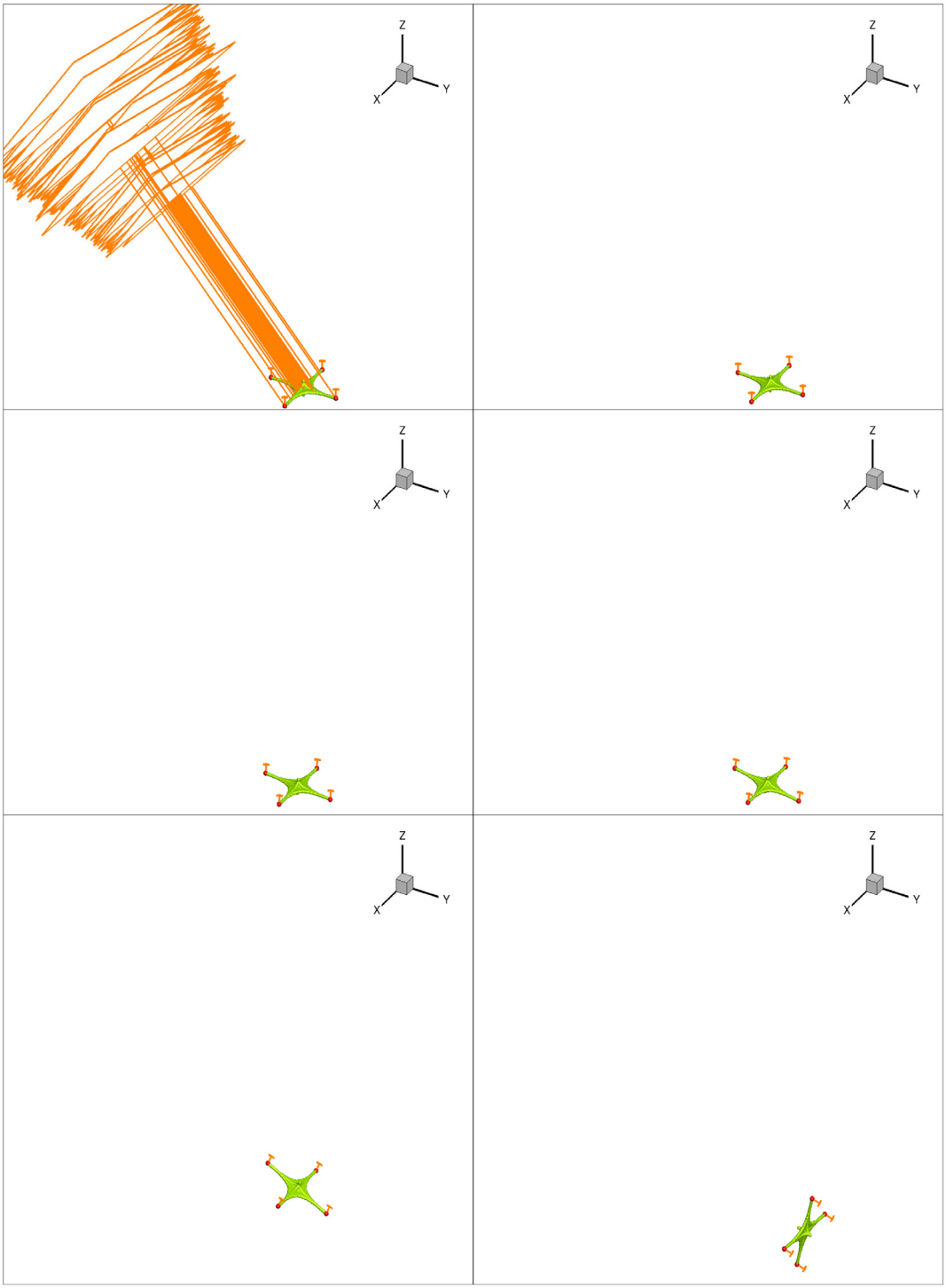

Fig. 7. Starting top left to bottom right: sequence of frames after an initial lateral distribution of pulses. The UAV starts to go into an uncontrollable spin. Breaking of the UAV is suppressed in this example.

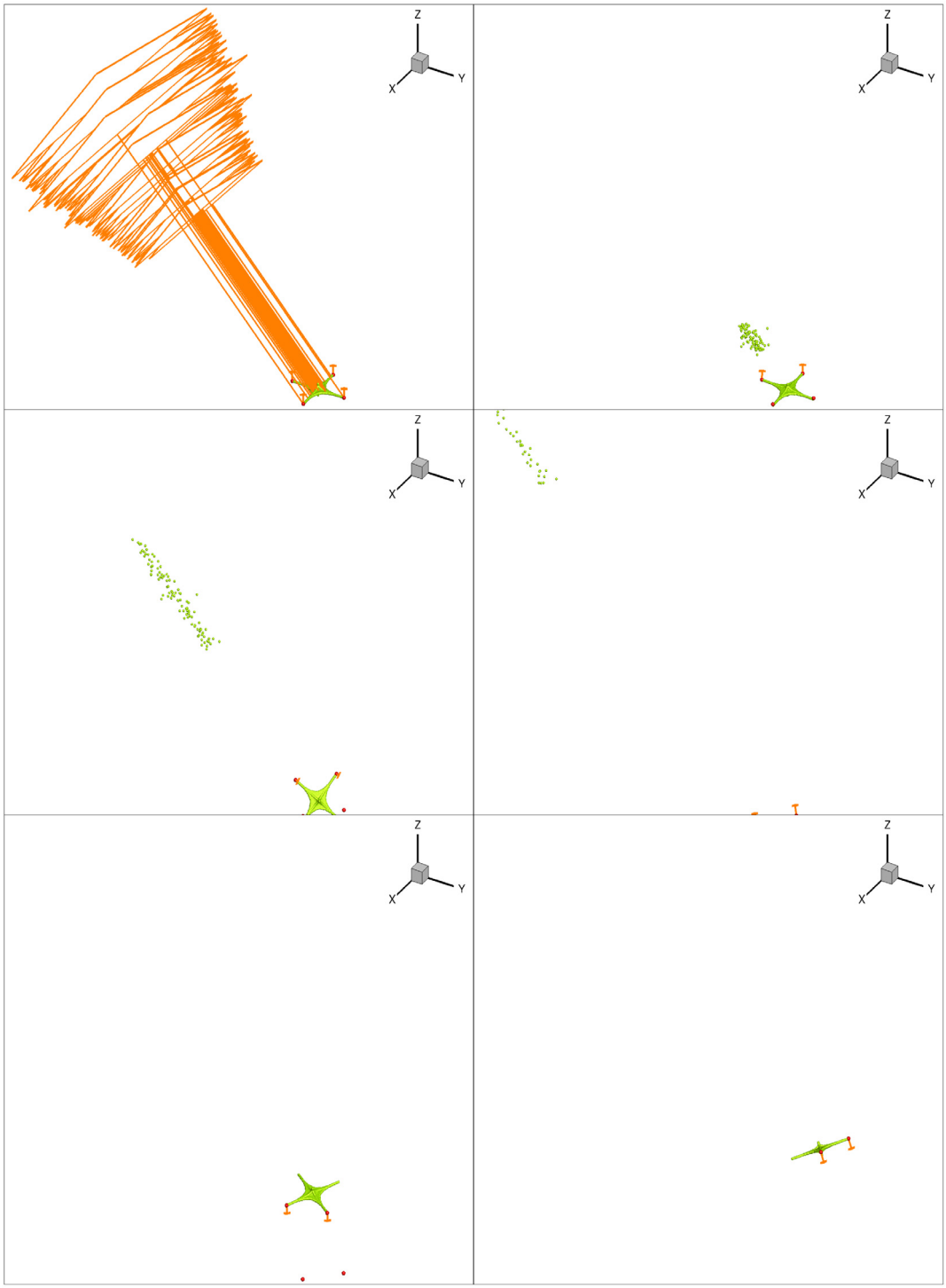

Fig. 8. Starting top left to bottom right: sequence of frames after an initial lateral distribution of pulses. The debris is dislodged and ejected and the UAV starts to go into an uncontrollable spin and breakup, much more quickly than in the first example with no breakup.

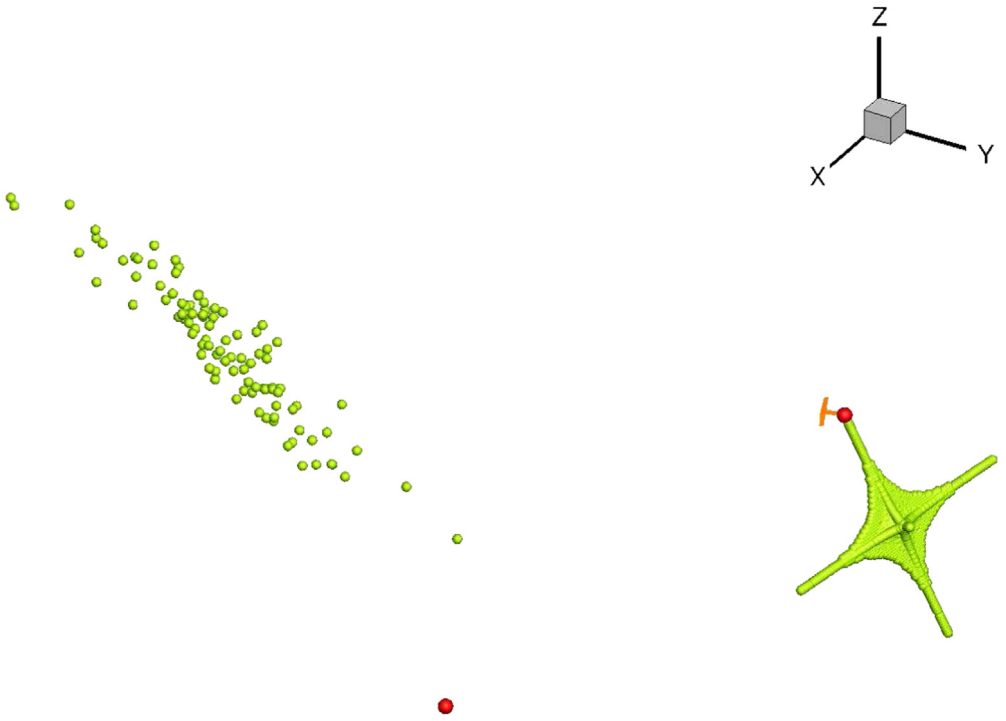

Fig. 9. Zoom on the last frame showing the dislodged debris. Due to the spiraling of the UAV, the debris gets "flung" in different directions, due to being dislodged and released with a combination of the impulse force and the last velocity when attached to the UAV.

multiple fragments from breakup/disintegration and shot-gun blast impact where the application of continuum approaches would be virtually impossible. The dynamics of fragments of clusters that evolve and interact with the quadcopter and other fragments is complex. Studies on cluster-to-cluster interaction can be found in Zohdi [2–7]. There is an extremely close area to this field, namely the study of "granular" or "particulate" media, for example see Duran [15], Pöschel and Schwager [16], Onate et al. [17,18], Rojek et al. [19], Carbonell et al. [20], Labra and Onate [21] and Zohdi [7].

3. **Composite materials and stress analysis:** The use of lightweight composite materials, such as ballistic fabric to enhance UAV resiliency leads to spatially heterogeneous criteria for spall and fragmentation. UAVs are typically constructed from lightweight composite materials and thermoplastics. In very high-end and military cases, ballistic fabric shielding is included (critical military and commercial structural components).[5] Furthermore, many of these UAVs are 3D printed with particle-functionalized/reinforced materials used in Additive Manufacturing. Specifically, *heated filament based materials* which are comprised of thermoplastics. Second-phase particles are added to the heated mixture which solidify (cure) to form the overall material properties comprised of particles in a binding matrix when deposited on a fabric substrate. The particles are used to "tune" the binding matrix properties to the desired overall material state. This makes the spall characteristics much more difficult, but presents itself as a next step in a more rigorous analysis. This will require a more detailed discretization of the propellors and motors.
4. **Multiple UAVs-swarms:** The scenario of a single UAV being shot down is quite complicated, and is further complicated by proposals of swarms of UAV's. The general topic of swarms has received considerable attention in the last few years, primarily because of the huge increase in the availability of small-scale Unmanned Airborne Vehicles (UAVs). Generally speaking, the term *swarm* is usually meant identify a collection of mobile interacting objects (agents) that can be programmed for a collective goal. This entails the dynamics of interacting UAVs, in addition to complex aerodynamics involving solid–fluid interaction. Small UAVs, such

[5] In aircraft applications, ballistic fabric shielding is universally employed to enhance the aircraft's protection from debris. The reader is referred to Tabiei and Nilakantan [22] for an exhaustive and comprehensive overview of all aspects of ballistic fabric.

a quadcopters, are usually battery powered. Thus, they have limited range and their paths must be planned carefully to conserve power. It has been proposed to used multiple UAV's working in tandem to map locations of interest. In this regard, multiple UAV agent-based "swarm" paradigms have been proposed. For example, Zohdi [12,13] has developed agent-based models for a team of swarm members to maximize mapped locations with various optimality constraints, such as minimum flight time or minimum energy usage. Simplified swarm modeling, as a set of interacting point masses dates back, at least, to Breder (1952) [23]. The usual approach to modeling such systems is to use a combination of short-range and long-range interaction forces (Gazi and Passino [24], Bender and Fenton [25], Kennedy and Eberhart [26] and Zohdi [12,13]). Early approaches that rely on decentralized organization can be found in Beni [27], Brooks [28], Dudek et al. [29], Cao et al. [30] and Liu and Passino [31]. However, there are alternative rule-driven swarms where the interaction is not governed by forces, but by proximal instructions such as: (a) if a fellow swarm agent gets close to me, attempt to retreat as far as possible, (b) follow the leader, (c) stay in clusters, etc. For example, ant colonies (Bonabeau et al., [32]) exhibit foraging-type behavior, in addition to the trail-laying-trail-following mechanism for finding food sources, where they deposit a chemical substance, called *pheromone*, which decays over time. The fellow swarm agents detect paths with a high pheromone concentration (where the food source is highly concentrated) and follow them (Kennedy and Eberhart [26] and Bonabeau et al. [32], Dorigo et al., [33], Bonabeau et al. [32], Bonabeau et al. [34] and Fiorelli et al. [35]). For certain swarms, the "visual field" of the individual agents may play a significant role, while in others, this is a non-issue, for example if the agents are robots or UAVs where the communication is electronic. Still, in some systems, agents interact with a specific set of swarm agents, *regardless* of whether they are far away (Feder [36]). For example, based on a number of careful observations, Starlings (Sturnus vulgaris), Ballerini et al. [37] conclude, that such birds communicate with a certain number of birds surrounding it, *regardless of the distance away*, attributing this to a perceptual limit in of the number of objects that they can track (the sixth or seventh nearest neighbor). These issues are currently under investigation by the author.

Acknowledgments

This work was funded in part by the Powley Foundation, the Pacific Earthquake Engineering Research Center (PEER) and the Army Research Laboratory through the Army High Performance Computing Research Center (cooperative agreement W911NF-07-2-0027).

Appendix A. Temporal discretization

Each particle's equation of motion is given by

$$m\dot{\mathbf{v}} = \boldsymbol{\Psi}, \tag{A.1}$$

where $\boldsymbol{\Psi}$ is the force provided from interactions with other particles the external environment. Expanding the velocity in a Taylor series about $t + \phi\Delta t$ we obtain $(0 \leq \phi \leq 1)$

$$\boldsymbol{v}(t+\Delta t) = \boldsymbol{v}(t+\phi\Delta t) + \frac{d\boldsymbol{v}}{dt}|_{t+\phi\Delta t}(1-\phi)\Delta t + \frac{1}{2}\frac{d^2\boldsymbol{v}}{dt^2}|_{t+\phi\Delta t}(1-\phi)^2(\Delta t)^2 + \mathcal{O}(\Delta t)^3 \tag{A.2}$$

and

$$\boldsymbol{v}(t) = \boldsymbol{v}(t+\phi\Delta t) - \frac{d\boldsymbol{v}}{dt}|_{t+\phi\Delta t}\phi\Delta t + \frac{1}{2}\frac{d^2\boldsymbol{v}}{dt^2}|_{t+\phi\Delta t}\phi^2(\Delta t)^2 + \mathcal{O}(\Delta t)^3. \tag{A.3}$$

Subtracting the two expressions yields

$$\frac{d\boldsymbol{v}}{dt}|_{t+\phi\Delta t} = \frac{\boldsymbol{v}(t+\Delta t) - \boldsymbol{v}(t)}{\Delta t} + \hat{\mathcal{O}}(\Delta t), \tag{A.4}$$

where $\hat{\mathcal{O}}(\Delta t) = \mathcal{O}(\Delta t)^2$ when $\phi = \frac{1}{2}$. Inserting this into the equation of motion yields

$$\boldsymbol{v}(t+\Delta t) = \boldsymbol{v}(t) + \frac{\Delta t}{m}\boldsymbol{\Psi}(t+\phi\Delta t) + \hat{\mathcal{O}}(\Delta t)^2. \tag{A.5}$$

Note that adding a weighted sum of Eqs. (A.2) and (A.3) yields

$$\boldsymbol{v}(t+\phi\Delta t) = \phi\boldsymbol{v}(t+\Delta t) + (1-\phi)\boldsymbol{v}(t) + \mathcal{O}(\Delta t)^2, \tag{A.6}$$

which will be useful shortly. Now expanding the position of the center of mass in a Taylor series about $t + \phi\Delta t$ we obtain

$$\boldsymbol{r}(t+\Delta t) = \boldsymbol{r}(t+\phi\Delta t) + \frac{d\boldsymbol{r}}{dt}|_{t+\phi\Delta t}(1-\phi)\Delta t + \frac{1}{2}\frac{d^2\boldsymbol{r}}{dt^2}|_{t+\phi\Delta t}(1-\phi)^2(\Delta t)^2 + \mathcal{O}(\Delta t)^3 \tag{A.7}$$

and

$$\boldsymbol{r}(t) = \boldsymbol{r}(t+\phi\Delta t) - \frac{d\boldsymbol{r}}{dt}|_{t+\phi\Delta t}\phi\Delta t + \frac{1}{2}\frac{d^2\boldsymbol{r}}{dt^2}|_{t+\phi\Delta t}\phi^2(\Delta t)^2 + \mathcal{O}(\Delta t)^3. \tag{A.8}$$

Subtracting the two expressions yields

$$\frac{\boldsymbol{r}(t+\Delta t) - \boldsymbol{r}(t)}{\Delta t} = \boldsymbol{v}(t+\phi\Delta t) + \hat{\mathcal{O}}(\Delta t). \tag{A.9}$$

Inserting Eq. (A.6) yields

$$\boldsymbol{r}(t+\Delta t) = \boldsymbol{r}(t) + (\phi\boldsymbol{v}(t+\Delta t) + (1-\phi)\boldsymbol{v}(t))\,\Delta t + \hat{\mathcal{O}}(\Delta t)^2 \tag{A.10}$$

and thus using Eq. (A.5) yields

$$\boldsymbol{r}(t+\Delta t) = \boldsymbol{r}(t) + \boldsymbol{v}(t)\Delta t + \frac{\phi(\Delta t)^2}{m}\boldsymbol{\Psi}(t+\phi\Delta t) + \hat{\mathcal{O}}(\Delta t)^2. \tag{A.11}$$

The term $\boldsymbol{\Psi}(t+\phi\Delta t)$ can be approximated by

$$\boldsymbol{\Psi}(t+\phi\Delta t) \approx \phi\,\boldsymbol{\Psi}(\boldsymbol{r}(t+\Delta t)) + (1-\phi)\,\boldsymbol{\Psi}(\boldsymbol{r}(t)), \tag{A.12}$$

yielding

$$\boldsymbol{r}(t+\Delta t) = \boldsymbol{r}(t) + \boldsymbol{v}(t)\Delta t + \frac{\phi(\Delta t)^2}{m}\left(\phi\,\boldsymbol{\Psi}(\boldsymbol{r}(t+\Delta t)) + (1-\phi)\,\boldsymbol{\Psi}(\boldsymbol{r}(t))\right) + \hat{\mathcal{O}}(\Delta t)^2. \tag{A.13}$$

We note that

- When $\phi = 1$, then this is the (implicit) Backward Euler scheme, which is very stable (very dissipative) and $\mathcal{O}(\Delta t)^2$ locally in time,
- When $\phi = 0$, then this is the (explicit) Forward Euler scheme, which is conditionally stable and $\mathcal{O}(\Delta t)^2$ locally in time,
- When $\phi = 0.5$, then this is the (implicit) "Midpoint" scheme, which is stable and $\hat{\mathcal{O}}(\Delta t)^2 = \mathcal{O}(\Delta t)^3$ locally in time.

Appendix B. Temporally adaptive iterative schemes

For illustration purposes, after time discretization of the acceleration term in the equations of motion $m\ddot{\mathbf{r}} = \boldsymbol{\Psi}$ using a ϕ-method

$$\boldsymbol{r}^{L+1} = \boldsymbol{r}^{L} + \boldsymbol{v}^{L}\Delta t + \frac{\phi(\Delta t)^2}{m}\left(\phi\,\boldsymbol{\Psi}(\boldsymbol{r}^{L+1}) + (1-\phi)\,\boldsymbol{\Psi}(\boldsymbol{r}^{L})\right), \tag{B.1}$$

one arrives at the following abstract form, for the entire system of particles,

$$\mathcal{A}(\boldsymbol{r}^{L+1}) = \mathcal{F}. \tag{B.2}$$

It is convenient to write

$$\mathcal{A}(\boldsymbol{r}^{L+1}) - \mathcal{F} = \mathcal{G}(\boldsymbol{r}^{L+1}) - \boldsymbol{r}^{L+1} + \mathcal{R} = \mathbf{0}, \tag{B.3}$$

where $\mathcal{R}$ is a remainder term that does not depend on the solution, i.e. $\mathcal{R} \neq \mathcal{R}(\boldsymbol{r}^{L+1})$. A straightforward iterative scheme can be written as

$$\boldsymbol{r}^{L+1,K} = \mathcal{G}(\boldsymbol{r}^{L+1,K-1}) + \mathcal{R}, \tag{B.4}$$

where $K = 1, 2, 3, \ldots$ is the index of iteration within time step $L+1$. The convergence of such a scheme is dependent on the behavior of $\mathcal{G}$. Namely, a sufficient condition for convergence is that $\mathcal{G}$ is a contraction mapping for all $\boldsymbol{r}^{L+1,K}$, $K = 1, 2, 3...$ In order to investigate this further, we define the iteration error as $\varepsilon^{L+1,K} \stackrel{\text{def}}{=} \boldsymbol{r}^{L+1,K} - \boldsymbol{r}^{L+1}$. A necessary restriction for convergence is iterative self consistency, i.e. the "exact" (discretized) solution must be represented by the scheme

$$\mathcal{G}(\boldsymbol{r}^{L+1}) + \mathcal{R} = \boldsymbol{r}^{L+1}. \tag{B.5}$$

Enforcing this restriction, a sufficient condition for convergence is the existence of a contraction mapping

$$\varepsilon^{L+1,K} = \|\boldsymbol{r}^{L+1,K} - \boldsymbol{r}^{L+1}\| = \|\mathcal{G}(\boldsymbol{r}^{L+1,K-1}) - \mathcal{G}(\boldsymbol{r}^{L+1})\| \tag{B.6}$$

$$\leq \eta^{L+1,K} \|\boldsymbol{r}^{L+1,K-1} - \boldsymbol{r}^{L+1}\|, \tag{B.7}$$

where, if $0 \leq \eta^{L+1,K} < 1$ for each iteration K, then $\varepsilon^{L+1,K} \rightarrow \boldsymbol{0}$ for any arbitrary starting value $\boldsymbol{r}^{L+1,K=0}$, as $K \rightarrow \infty$. This type of contraction condition is sufficient, but not necessary, for convergence. Inserting this into $m\ddot{\mathbf{r}} = \boldsymbol{\Psi}(\boldsymbol{r})$ leads to

$$\boldsymbol{r}^{L+1,K} = \underbrace{\boldsymbol{r}^{L} + \boldsymbol{v}^{L}\Delta t + \frac{\phi(\Delta t)^2}{m}\left((1-\phi)\,\boldsymbol{\Psi}(\boldsymbol{r}^{L})\right)}_{\mathcal{R}} + \underbrace{\frac{\phi(\Delta t)^2}{m}\left(\phi\,\boldsymbol{\Psi}(\boldsymbol{r}^{L+1,K-1})\right)}_{\mathcal{G}(\boldsymbol{r}^{L+1,K-1})}, \tag{B.8}$$

whose convergence is restricted by $\eta \propto \frac{(\phi\Delta t)^2}{m}$. Therefore, we see that the contraction constant of $\mathcal{G}$ is (1) directly dependent on the strength of the interaction forces, (2) inversely proportional to m and (3) directly proportional to $\phi\Delta t$. Therefore, if convergence is slow within a time step, the time step size, which is adjustable, can be reduced by an appropriate amount to increase the rate of convergence. Thus, decreasing the time step size improves the convergence, however, we want to simultaneously maximize the time-step sizes to decrease overall computing time, while still meeting an error tolerance on the numerical solution's accuracy. In order to achieve this goal, we follow an approach found in Zohdi [2–7,12–14] originally developed for continuum thermo-chemical multifield problems in which (1) one approximates

$$\eta^{L+1,K} \approx S(\Delta t)^p \tag{B.9}$$

(S is a constant) and (2) one assumes that the error within an iteration to behave according to

$$(S(\Delta t)^p)^K \varepsilon^{L+1,0} = \varepsilon^{L+1,K}, \tag{B.10}$$

$K = 1, 2, \ldots$, where $\varepsilon^{L+1,0}$ is the initial norm of the iterative error and S is intrinsic to the system.[6] Our goal is to meet an error tolerance in exactly a preset number of iterations. To this end, one writes

$$(S(\Delta t_{\text{tol}})^p)^{K_d} \varepsilon^{L+1,0} = TOL, \tag{B.11}$$

where TOL is a tolerance and where K_d is the number of desired iterations.[7] If the error tolerance is not met in the desired number of iterations, the contraction constant $\eta^{L+1,K}$ is too large. Accordingly, one can solve for a new smaller step size, under the assumption that S is constant,

$$\Delta t_{\text{tol}} = \Delta t \left(\frac{(\frac{TOL}{\varepsilon^{L+1,0}})^{\frac{1}{pK_d}}}{(\frac{\varepsilon^{L+1,K}}{\varepsilon^{L+1,0}})^{\frac{1}{pK}}} \right). \tag{B.12}$$

The assumption that S is constant is not critical, since the time steps are to be recursively refined and unrefined throughout the simulation. Clearly, the expression in Eq. (B.12) can also be used for time step enlargement, if

[6] For the class of problems under consideration, due to the quadratic dependency on Δt, $p \approx 2$.

[7] Typically, K_d is chosen to be between five to ten iterations.

convergence is met in less than K_d iterations.[8] An implementation of the procedure is as follows:

$$
\begin{array}{l}
(1)\,\text{GLOBAL FIXED} - \text{POINT ITERATION : (SET i} = 1 \text{ AND K} = 0) : \\
(2)\,\text{IF i} > \text{N}_\text{p} \text{ THEN GO TO (4)} \\
(3)\,\text{IF i} \leq \text{N}_\text{p} \text{ THEN :} \\
\quad (a)\ \text{COMPUTE POSITION :} \boldsymbol{r}_i^{L+1,K} \\
\quad (b)\ \text{GO TO (2) FOR NEXT PARTICLE (i} = \text{i} + 1) \\
(4)\,\text{ERROR MEASURE :} \\
\quad (a) \varepsilon_K \overset{\text{def}}{=} \dfrac{\sum_{i=1}^{N_p} \| \boldsymbol{r}_i^{L+1,K} - \boldsymbol{r}_i^{L+1,K-1} \|}{\sum_{i=1}^{N_p} \| \boldsymbol{r}_i^{L+1,K} - \boldsymbol{r}_i^{L} \|} \qquad \text{(normalized)} \\
\quad (b) Z_K \overset{\text{def}}{=} \dfrac{\varepsilon_K}{TOL_r} \\
\quad (c) \Phi_K \overset{\text{def}}{=} \left(\dfrac{(\frac{TOL}{\varepsilon_0})^{\frac{1}{pK_d}}}{(\frac{\varepsilon_K}{\varepsilon_0})^{\frac{1}{pK}}} \right) \\
(5)\underline{\text{IF TOLERANCE MET } (Z_K \leq 1) \text{ AND } K < K_d \text{ THEN :}} \\
\quad (a)\ \text{INCREMENT TIME : } t = t + \Delta t \\
\quad (b)\ \text{CONSTRUCT NEW TIME STEP : } \Delta t = \Phi_K \Delta t, \\
\quad (c)\ \text{SELECT MINIMUM : } \Delta t = MIN(\Delta t^{lim}, \Delta t) \text{ AND GO TO (1)} \\
(6)\underline{\text{IF TOLERANCE NOT MET } (Z_K > 1) \text{ AND } K = K_d \text{ THEN :}} \\
\quad (a)\ \text{CONSTRUCT NEW TIME STEP :} \Delta t = \Phi_K \Delta t \\
\quad (b)\ \text{RESTART AT TIME} = \text{t AND GO TO (1)}
\end{array}
\tag{B.13}
$$

Generally speaking, the iterative error, which is a function of the time step size, is temporally variable and can become stronger, weaker, or possibly oscillatory, is extremely difficult to ascertain a-priori as a function of the time step size. Therefore, to circumvent this problem, the adaptive strategy presented in this section was developed to provide accurate solutions by iteratively adjusting the time steps. Specifically, a sufficient condition for the convergence of the presented fixed-point scheme was that the spectral radius or contraction constant of the coupled operator, which depends on the time step size, must be less than unity. This observation was used to adaptively maximize the time step sizes, while simultaneously controlling the coupled operator's spectral radius, in order to deliver solutions below an error tolerance within a prespecified number of desired iterations. This recursive staggering error control can allow for substantial reduction of computational effort by the adaptive use of large time steps. Furthermore, such a recursive process has a reduced sensitivity, relative to an explicit staggering approach, to the order in which the individual equations are solved, since it is self-correcting.

Remark. With regard to the solution process, a recursive iterative scheme of the Jacobi-type, where the updates are made only after one complete system iteration, was illustrated in the derivations only for algebraic simplicity. The Jacobi method is easier to address theoretically, while the Gauss–Seidel type method, which involves immediately using the most current values, when they become available, is usually used at the implementation level. As is well-known, under relatively general conditions, if the Jacobi method converges, the Gauss–Seidel method converges at a faster rate, while if the Jacobi method diverges, the Gauss–Seidel method diverges at a faster rate (for example, see Ames [38] or Axelsson [39]). It is important to realize that the Jacobi method is perfectly parallelizable. In other words, the calculation for each particle are uncoupled, with the updates only coming afterward. Gauss–Seidel, since it requires the most current updates, couples the particle calculations immediately. However, these methods can be combined to create hybrid approaches, whereby the entire particulate flow is partitioned into groups and within each group a Gauss–Seidel method is applied. In other words, for a group, the positions of any particles from outside are

[8] Time-step size adaptivity is important, since the system's dynamics can dramatically change over the course of time, possibly requiring quite different time step sizes to control the iterative error. However, to maintain the accuracy of the time-stepping scheme, one must respect an upper bound dictated by the discretization error, i.e., $\Delta t \leq \Delta t^{lim}$.

initially frozen, as far as calculations involving members of the group are concerned. After each isolated group's solution (particle positions) has converged, computed in parallel, then all positions are updated, i.e. the most current positions become available to all members of the swarm, and the isolated group calculations are repeated. Classical solution methods require $\mathcal{O}(N^3)$ operations, whereas iterative schemes, such as the one presented, typically require order N^q, where $1 \leq q \leq 2$. For details see Axelsson [39]. Also, such solvers are highly advantageous since solutions to previous time steps can be used as the first guess to accelerate the solution procedure.

References

[1] D. Powell, T.I. Zohdi, Attachment mode performance of network-modeled ballistic fabric shielding, Composites B 40 (6) (2009) 451–460.
[2] T.I. Zohdi, Numerical simulation of charged particulate cluster-droplet impact on electrified surfaces, J. Comput. Phys. 233 (2013) 509–526.
[3] T.I. Zohdi, A direct particle-based computational framework for electrically-enhanced thermo-mechanical sintering of powdered materials, Math. Mech. Solids (2014) 1–21. http://dx.doi.org/10.1007/s11831-013-9092-6.
[4] T.I. Zohdi, Charge-induced clustering in multifield particulate flow, Internat. J. Numer. Methods Engrg. 62 (7) (2005) 870–898.
[5] T.I. Zohdi, Computation of strongly coupled multifield interaction in particle-fluid systems, Comput. Methods Appl. Mech. Engrg. 196 (2007) 3927–3950.
[6] T.I. Zohdi, On the dynamics of charged electromagnetic particulate jets, Arch. Comput. Methods Eng. 17 (2) (2010) 109–135.
[7] T.I. Zohdi, Dynamics of charged particulate systems, in: Modeling, Theory and Computation, Springer-Verlag, 2012.
[8] M.W. Mueller, R. D'Andrea, Relaxed hover solutions for multicopters: application to algorithmic redundancy and novel vehicles, Int. J. Robot. Res. 35 (8) (2015) 873–889.
[9] M.W. Mueller, R. D'Andrea, Stability and control of a quadrocopter despite the complete loss of one, two, or three propellers, in: IEEE International Conference on Robotics and Automation, ICRA, 2014.
[10] M. Hehn, R. Ritz, R. D Andrea, Performance benchmarking of quadrotor systems using time-optimal control, Auton. Robots 33 (1–2) (2012) 69–88.
[11] B. Houska, H. Ferreau, M. Diehl, ACADO toolkit: An open source framework for automatic control and dynamic optimization, Optim. Control Appl. Methods 32 (3) (2011) 298–312.
[12] T.I. Zohdi, Computational design of swarms, Internat. J. Numer. Methods Engrg. 57 (2003) 2205–2219.
[13] T.I. Zohdi, Mechanistic modeling of swarms, Comput. Methods Appl. Mech. Engrg. 198 (21–26) (2009) 2039–2051.
[14] T.I. Zohdi, An adaptive-recursive staggering strategy for simulating multifield coupled processes in microheterogeneous solids, Internat. J. Numer. Methods Engrg. 53 (2002) 1511–1532.
[15] J. Duran, Sands, Powders and Grains. An Introduction to the Physics of Granular Matter, Springer Verlag, 1997.
[16] T. Pöschel, T. Schwager, Computational Granular Dynamics, Springer Verlag, 2004.
[17] E. Onate, S.R. Idelsohn, M.A. Celigueta, R. Rossi, Advances in the particle finite element method for the analysis of fluid-multibody interaction and bed erosion in free surface flows, Comput. Methods Appl. Mech. Engrg. 197 (19–20) (2008) 1777–1800.
[18] E. Onate, M.A. Celigueta, S.R. Idelsohn, F. Salazar, B. Suárez, Possibilities of the particle finite element method for fluid-soil–structure interaction problems, Comput. Mech. 48 (2011) 307–318.
[19] J. Rojek, C. Labra, O. Su, E. Onate, Comparative study of different discrete element models and evaluation of equivalent micromechanical parameters, Int. J. Solids Struct. 49 (2012) 1497–1517. http://dx.doi.org/10.1016/j.ijsolstr.2012.02.032.
[20] J.M. Carbonell, E. Onate, B. Suarez, Modeling of ground excavation with the particle finite element method, ASCE J. Eng. Mech. 136 (2010) 455–463.
[21] C. Labra, E. Onate, High-density sphere packing for discrete element method simulations, Commun. Numer. Methods. Eng. 25 (7) (2009) 837–849.
[22] A. Tabiei, G. Nilakantan, Ballistic impact of dry woven fabric composites: a review, Appl. Mech. Rev. 61 (2008) (2008) 1–13.
[23] C.M. Breder, Equations descriptive of fish schools and other animal aggregations, Ecology 35 (3) (1954) 361–370.
[24] V. Gazi, K.M. Passino, Stability analysis of swarms, in: Proceedings of the American Control Conference, Anchorage, AK May 8–10, 2010.
[25] J. Bender, R. Fenton, On the flow capacity of automated highways, Transp. Sci. 4 (1970) 52–63.
[26] J. Kennedy, R. Eberhart, Swarm Intelligence, Morgan Kaufmann Publishers, 2001.
[27] G. Beni, The concept of cellular robotic system, in: IEEE International Symposium on Intelligent Control, 1988, pp. 57–62.
[28] R.A. Brooks, Intelligence without reason, in: Proceedings of the International Joint Conference on Artificial Intelligence, IJCAI-91, 1991, pp. 569–595.
[29] G. Dudek, M. Jenkin, E. Milios, D. Wilkes, A taxonomy for multi-agent robotics, Auton. Robots 3 (1996) 375–397.
[30] Y.U. Cao, A.S. Fukunaga, A. Kahng, Cooperative mobile robotics: Antecedents and directions, Auton. Robots 4 (1) (1997) 7–27.
[31] Y. Liu, K.M. Passino, Swarm Intelligence: Literature Overview, Technical Report, Ohio State University, 2000.
[32] E. Bonabeau, M. Dorigo, G. Theraulaz, Swarm Intelligence: From Natural to Artificial Systems, Oxford University Press, New York, 1999.
[33] M. Dorigo, V. Maniezzo, A. Colorni, Ant system: optimization by a colony of cooperating agents, IEEE Trans. Syst. Man Cybern. B 26 (1) (1996) 29–41.
[34] E. Bonabeau, C. Meyer, Swarm intelligence: A whole new way to think about business, Harv. Bus. Rev. 79 (5) (2001) 106–114.
[35] E. Fiorelli, N.E. Leonard, P. Bhatta, D. Paley, R. Bachmayer, D.M. Fratantoni, Multi-auv control and adaptive sampling in monterey bay, in: Autonomous Underwater Vehicles, 2004 IEEE/OES, 2004, pp. 134–147.

[36] T. Feder, Statistical physics is for the birds, Phys. Today (2007) 28–29.
[37] M. Ballerini, N. Cabibbo, R. Candelier, A. Cavagna, E. Cisbani, I. Giardina, V. Lecomte, A. Orlandi, G. Parisi, A. Procaccini, M. Viale, V. Zdravkovic, Interaction ruling animal collective behavior depends on topological rather than metric distance: evidence from a field study, Proc. Natl. Acad. Sci. USA 105 (4) (2008) 1232–1237.
[38] W.F. Ames, Numerical Methods for Partial Differential Equations, Academic Press, 1977.
[39] O. Axelsson, Iterative Solution Methods, Cambridge University Press, 1994.